



A theoretical investigation of the effect of proliferation and adhesion on monoclonal conversion in the colonic crypt

Gary R. Mirams ^{a,*}, Alexander G. Fletcher ^{b,c,1}, Philip K. Maini ^{b,c}, Helen M. Byrne ^{a,d}

^a Computational Biology, Department of Computer Science, University of Oxford, Parks Road, Oxford OX1 3QD, UK

^b Centre for Mathematical Biology, Mathematical Institute, University of Oxford, St. Giles', Oxford OX1 3LB, UK

^c Oxford Centre for Integrative Systems Biology, Department of Biochemistry, University of Oxford, South Parks Road, Oxford OX1 3QU, UK

^d Oxford Centre for Collaborative Applied Mathematics, Mathematical Institute, University of Oxford, St. Giles', Oxford OX1 3LB, UK

HIGHLIGHTS

- We use a spatial cell-based model to study monoclonal conversion in the crypt.
- Mutations are introduced with varied height, proliferation and adhesion.
- Mutations occurring more than one cell from the crypt base rarely dominate.
- Changes to adhesion can significantly affect probability of domination.
- Changes to proliferation cause non-linear changes to the probability of domination.

ARTICLE INFO

Article history:

Received 31 March 2012

Received in revised form

24 July 2012

Accepted 2 August 2012

Available online 10 August 2012

Keywords:

Mathematical model

Colorectal crypt

Stem cell

Mutation

Clonal expansion

ABSTRACT

The surface epithelium lining the intestinal tract renews itself rapidly by a coordinated programme of cell proliferation, migration and differentiation events that is initiated in the crypts of Lieberkühn. It is generally believed that colorectal cancer arises due to mutations that disrupt the normal cellular dynamics of the crypts. Using a spatially structured cell-based model of a colonic crypt, we investigate the likelihood that the progeny of a mutated cell will dominate, or be sloughed out of, a crypt. Our approach is to perform multiple simulations, varying the spatial location of the initial mutation, and the proliferative and adhesive properties of the mutant cells, to obtain statistical distributions for the probability of their domination. Our simulations lead us to make a number of predictions. The process of monoclonal conversion always occurs, and does not require that the cell which initially gave rise to the population remains in the crypt. Mutations occurring more than one to two cells from the base of the crypt are unlikely to become the dominant clone. The probability of a mutant clone persisting in the crypt is sensitive to dysregulation of adhesion. By comparing simulation results with those from a simple one-dimensional stochastic model of population dynamics at the base of the crypt, we infer that this sensitivity is due to direct competition between wild-type and mutant cells at the base of the crypt. We also predict that increases in the extent of the spatial domain in which the mutant cells proliferate can give rise to counter-intuitive, non-linear changes to the probability of their fixation, due to effects that cannot be captured in simpler models.

© 2012 Elsevier Ltd. All rights reserved.

1. Introduction

The intestinal epithelium is one of the most rapidly renewing mammalian tissues, with complete turnover occurring every 2–3 days in mice and 3–5 days in humans (Okamoto and Watanabe, 2004; Ross et al., 2003). About 2×10^7 crypts of Lieberkühn form

the epithelial layer of the human large intestine (Potten et al., 2003). Topologically, crypts are 'test tube' or 'flask'-shaped invaginations in the epithelium of the colon, providing a huge surface area for the absorption of water. Cells towards the base of the crypts proliferate. As cells ascend the crypt walls they cease proliferation and differentiate into specialised absorptive or secretory cells. At the crypt orifice, differentiated cells undergo apoptosis and are shed into the intestinal lumen (Bullen et al., 2006). Cell migration up the crypt is thought to be driven by mitotic activity, the increase in cell number creating a passive, pressure-driven cell movement, but may also be influenced by active cell movement, active basement membrane

* Corresponding author. Tel.: +44 1865 610671.

E-mail address: gary.mirams@cs.ox.ac.uk (G.R. Mirams).

¹ Joint first authors.

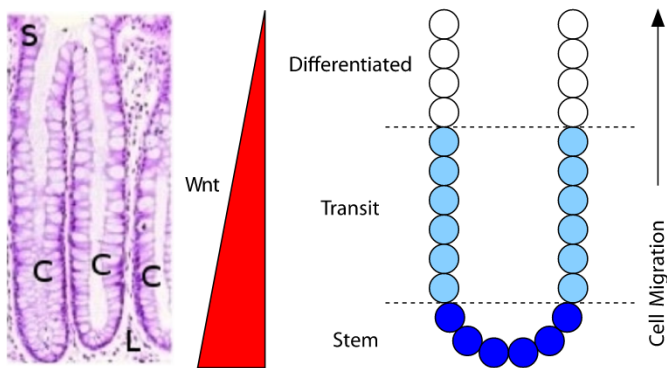


Fig. 1. Left: hematoxylin and eosin stained section through normal healthy human colonic mucosae, showing the test-tube like structure of each crypt. Labels show surface epithelium (S), crypts (C) and the lamina propria separating them (L). Image reproduced from Shih et al. (2001), copyright (2001) National Academy of Sciences, USA. Right: diagram indicating the spatial location of the stem, transit amplifying and differentiated cell compartments within the crypt. A Wnt gradient up the crypt is hypothesised to regulate cell proliferation.

flow and cell shedding at the lumen (Wright and Alison, 1984a; Kaur and Potten, 1986). A histological image and a schematic of a normal healthy colonic crypt are shown in Fig. 1.

Due to the geometry and pattern of proliferation within a crypt, cells at its base typically give rise to the entire crypt population, as they divide and generate lineages of daughter cells (Barker et al., 2007). In this introduction, we consider the underlying regulation of this proliferation patterning in the crypt, and explain how cellular mutations are thought to cause dysregulation.

It has been proposed that a spatial gradient of extracellular Wnt factors along the crypt axis determines the position-dependent rates of cell proliferation, differentiation and death (Gaspar and Fodde, 2004). Activation of the canonical Wnt pathway is initiated when secreted Wnt glycoproteins bind to receptors on the cell membrane. The resulting complex triggers a signalling cascade, which causes the rate of degradation of the protein β -catenin to decrease. β -catenin can then accumulate, producing two major effects.

First, β -catenin localises to the nucleus, binds to transcription factors and induces the transcription of many Wnt target genes² (Pinto et al., 2003). These targets regulate crypt organisation in several ways, controlling (or influencing) proliferation, differentiation, adhesion and migration. Second, at the cell membrane β -catenin binds directly to components of adherens junctions (Perez-Moreno et al., 2003; Nelson and Nusse, 2004). Each of these behaviours has been significantly affected in knockout experiments targeting Wnt pathway components and downstream genes (van de Wetering et al., 2002; Sansom et al., 2007). For example, knock-outs of components of the pathway have been shown to halt completely migration of crypt cells, and to cause an increase in levels of proliferation (Sansom et al., 2004). This suggests that Wnt is a major controlling factor of cellular crypt dynamics. In support of this, mutations in key components of the Wnt pathway within epithelial crypt cells contribute to the initiation of over 90% of colorectal cancers, including most hereditary cases (Powell et al., 1992; Morin et al., 1997; Sparks et al., 1998; Ilyas, 2005; Barker et al., 2008). In this paper, we will simulate the mutation of single cells in the crypt, varying their proliferative and adhesive properties, along with the

initial spatial location of the mutation, in order to predict the probability that such mutants will dominate a colonic crypt.

As a crypt is a complex, highly regulated system, a theoretical approach is useful for gaining mechanistic insights into dynamics that cannot be readily measured. Mathematical modelling has been used to investigate aspects of colorectal cancer for over half a century. But only over the last 10–20 years has the quality of experimental data advanced sufficiently to warrant the development of detailed models of the cell population dynamics within the crypt. These include deterministic compartmental models formulated as systems of ordinary differential equations, such as those proposed by Johnston et al. (2007) and Boman et al. (2008), stochastic models such as those developed by Loeffler et al. (1993) and Komarova and Wang (2004), and more recent hybrid models such as those by Meineke et al. (2001), van Leeuwen et al. (2009), Osborne et al. (2010) and Fletcher et al. (2012). Other models focus on the sub-cellular behaviour of normal and mutant crypt cells (van Leeuwen et al., 2007; Mirams et al., 2010), or some of the later steps in colorectal carcinogenesis (Drasdo and Loeffler, 2001; Edwards and Chapman, 2007). In another recent theoretical study, Buske et al. (2011) developed a rule-based spatial model, which incorporates the effects of Wnt and Notch signalling on cell proliferative behaviour as well as explicit representation of the basement membrane that provides mechanical support to the crypt. To our knowledge, to date no theoretical investigation has yet been performed to determine how the probability of crypt domination by a mutant population depends on the spatial location of the initial mutation, and the proliferative and adhesive properties of the mutant cells.

The modular nature of the implementation of van Leeuwen et al.'s model of the crypt (van Leeuwen et al., 2009) enables us easily to use the Chaste platform (Cancer, Heart And Soft Tissue Environment, Pitt-Francis et al. (2009)) to perform large numbers of *in silico* experiments. Having studied the dynamics of a normal crypt, a next step is to consider the aberrant behaviour that arises when crypt cells accumulate genetic mutations. In this paper we will investigate crypt homeostasis and how it is disrupted by mutations that affect cell proliferation and/or adhesion (some of the primary effects of Wnt pathway mutations found in colorectal cancer). In each case, we will compute the probability that a mutant population fixates in the crypt, and how this probability depends on the spatial location of the initial mutation in the crypt. We will also compare our simulation results with those from a simple one-dimensional (1D) stochastic model of population dynamics at the base of the crypt, in order to determine the extent to which a simpler model can accurately capture the competition between normal and mutant clones observed in our cell-based simulations. The rest of the paper is organised as follows. In Section 2 we describe the mathematical model that is used to represent the colonic crypt and the simulations which we have performed. In Section 3 we present the results of these simulations, and we conclude in Section 4 with a summary of our findings and suggestions for future work.

2. Multiscale crypt model

Our model of a colonic crypt has been described in detail previously (van Leeuwen et al., 2009; Pitt-Francis et al., 2009), but we re-introduce it here. We simulate the dynamics of individual cells, whose movement is governed by a model of mechanical interactions (Section 2.1). The proliferative state of each cell is governed by a cell-cycle model, which takes into account the local Wnt stimulus (Section 2.2). For this study, the mechanical and proliferative properties of the cells may be altered under

² See <http://www.stanford.edu/~rnusse/pathways/targets.html> for an up-to-date list of target genes.

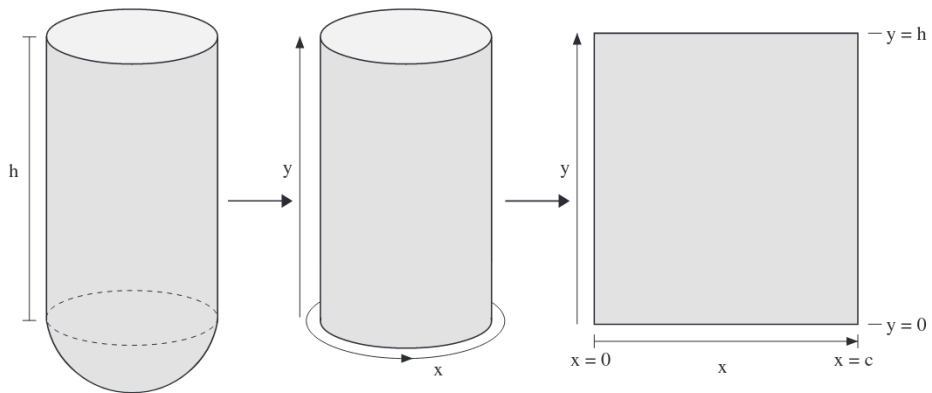


Fig. 2. Diagram indicating the geometric simplification and coordinates used in our model. We approximate the crypt by a cylinder and for convenience ‘unroll’ this onto a flat planar domain with periodic left- and right-hand boundaries.

mutations (Sections 2.3 and 2.4). Finally, we will describe the computational implementation of the simulations (Section 2.5).

2.1. Mechanical model and geometry

A variety of approaches can be used to model the mechanical behaviour of individual cells in a tissue. There are two basic components to any such model: the first step is to decide which cells are neighbours, and the second is to determine the forces transmitted by these neighbours. We adopt the tessellation-based, cell-centre approach of van Leeuwen et al. (2009), in which cells are defined by the location of their centres. Cell movement is determined by assuming that each cell exerts a linear spring force on its neighbours, this force acting parallel to the vector connecting their centres. Neighbours are defined by a Delaunay triangulation of the cell centres, which is updated at each time step. Movement is assumed to be highly viscous or ‘over-damped’; that is, we neglect inertial terms. Balancing the linear spring forces on an individual cell, with a drag term representing cell–substrate adhesion, the following equation of motion for the centre of cell i is obtained:

$$\frac{\alpha_i \eta}{\mu} \frac{d\mathbf{r}_i}{dt} = \sum_{j \in S_i} (\|\mathbf{r}_j - \mathbf{r}_i\| - s_{ij}(t)) \frac{(\mathbf{r}_j - \mathbf{r}_i)}{\|\mathbf{r}_j - \mathbf{r}_i\|} \quad (1)$$

where \mathbf{r}_i denotes the position of the centre of cell i , \mathbf{r}_j that of neighbouring cell j , $s_{ij}(t)$ is the equilibrium length of the spring connecting cells i and j at time t , S_i is the set of cells that are adjacent to cell i (in the Delaunay triangulation), μ is the spring constant, η the drag coefficient and α_i a scaling factor characterizing how the movement of mutant cells differs from that of normal cells. Thus we fix $\alpha_i = 1$ for wild-type cells. We assume that all progenies of a given mutant cell share the same value $\alpha_i \equiv \alpha$, which we refer to hereafter as the *adhesion scaling parameter*.

As noted by Meineke et al. (2001), the ratio η/μ can be written as a single parameter λ , which has units of time. A large value of λ corresponds to a long timescale for mechanical relaxation. We follow our previous study (van Leeuwen et al., 2009) by fixing $\lambda = 120$ s in all simulations, as in wild-type crypts this results in cells migrating up the crypt over the experimentally observed time-scales.

Following Meineke et al. (2001) and van Leeuwen et al. (2009), we have adopted a fixed cylindrical representation of the crypt, defined by the spatial domain

$$\{(x, y) \in \mathbb{R}^2 : 0 \leq x \leq c, 0 \leq y \leq h\},$$

where c and h denote the fixed circumference and height of the crypt, respectively, and periodicity is imposed at the left- and right-hand boundaries $x=0$ and $x=c$. This geometric simplification is illustrated in Fig. 2.

We restrict cells to lie on this fixed surface, and thus assume that planar cell polarity during mitosis and movement within the crypt is such that the epithelium remains as a monolayer. In particular, we do not allow the structure of the crypt to deform by processes such as uncontrolled proliferation: modelling crypt deformation is not the focus of this study, although it is the subject of active research (Dunn et al., 2012a).

An obvious limitation of our cylindrical representation of the crypt is that in practice crypts are test-tube-shaped. By simplifying the bottom of the crypt, we neglect effects such as cells passing from one side of the crypt to the other via the base of the crypt. Nonetheless, the cylindrical geometry is likely to be a reasonable approximation over much of the crypt height, as evidenced by the observation by Snippert et al. (2010) that few, if any, cell divisions lead to clonal expansion through the base to the opposite side of the crypt. We note also that our geometric approximation overestimates the number of cells at the crypt base, which means that the persistence times and probabilities of domination reported in Section 3 may be overestimates, as discussed by Fletcher et al. (2012). However, it is the variation in the qualitative behaviour of the system as the model parameters vary that is of interest in this work, and we envisage that the nature of these relationships will be preserved for more detailed geometries such as those considered by Buske et al. (2011) and Fletcher et al. (2012).

A no-flux boundary condition is imposed at the bottom of the domain ($y=0$), since cells cannot be pushed out of the base of the crypt. This condition is implemented as follows. We do not pin cells at the base of the crypt, but allow them to move in response to the mechanical forces they experience. Any cell centre pushed off the bottom of the domain is moved to a new position located a random distance, uniformly distributed between 0 and 0.05 cell diameters, above $y=0$. Cells that reach the top of the crypt are removed from the simulation, replicating sloughing. The average number of cells in histological sections, from the large bowel of mice (Sunter et al., 1979, Table 1, site (iii)), is approximately 16 cells in circumference and 20 cells in length. Our simulated crypt has dimensions 14 ‘relaxed cell diameters’ in circumference and 17 in height, thus we take $c=14$ and $h=17$. It should be noted that due to the increased proliferation (and therefore packing) in the base of the crypt, numbers of cells in typical, quasi-steady cross-sections from simulated crypts match those from histology.

A forward Euler discretisation of equation (1) with time-step Δt is used to calculate the new location of each cell. The same

time-step Δt is used to update the position of each cell in a simulation. Note that a smaller time-step is required for simulations in which the mutant population experiences lower cell-substrate adhesion than the wild-type cells (where $\alpha = 1$); we found that a time-step of

$$\Delta t = 30 \text{ s} \times \min(1, \alpha)$$

was sufficient to ensure numerical stability. After each round of cell movements we progress each cell through its cell cycle, allowing cells to divide when necessary (see next section), and removing cells when they move above the top of the crypt ($y=h$). After updating the location of each cell, we recalculate cell neighbours by re-meshing. Further details on the implementation can be found in Mirams (2008) and Pitt-Francis et al. (2009).

2.2. Cell-cycle model

We have formulated a simple model of Wnt-dependent cell proliferation. Our crypts consist of proliferating and non-proliferating cells, the former encompassing stem and transit cells and the latter corresponding to differentiated cells (see Fig. 1). Following van Leeuwen et al. (2009), we represent the Wnt gradient by a fixed external stimulus, whose non-dimensional concentration W decreases linearly from 1 at the crypt base to 0 at the top of the crypt (Gregorjeff and Clevers, 2005).

Near the base of the crypt, where cells are exposed to high levels of Wnt, we suppose the production of Wnt-dependent cell-cycle control proteins is enhanced and cells progress through the cell cycle. Towards the top of the crypt, where Wnt levels fall below a division threshold W_{thr} , cell division stops and cells are considered to be differentiated. We do not consider ‘contact inhibition’ of cell division, by which proliferation might be limited at high cell densities/pressures (Dietrich et al., 2002).

We choose W_{thr} so that the number of proliferative cells (and crypt turnover) in a healthy crypt matches experimental observations (Sunter et al., 1979; Wright and Alison, 1984b). For healthy cells the value of this division threshold is set to be $W_{\text{thr}} = 0.65$, so cells proliferate to 35% of the height of the crypt; we term this threshold height the *proliferation ceiling*, and denote it by y_{thr} .

It is important to include an element of stochasticity into the cell cycle duration in order to prevent the unrealistic situation where all cells divide synchronously (as we will see, this would always happen, regardless of the initial conditions). Following Meineke et al. (2001), we attribute stochastic variation to variation in the length of the G_1 phase only. Each proliferating cell is given a G_1 phase duration sampled from a normal distribution $N(9.4, 1)$ h (in practice, we truncate this distribution to ensure strictly positive times); with other cell cycle phases of $S=7.4$ h, $G_2=1.4$ h and $M=0.72$ h (the cell cycle times from region 3 of mouse large bowel in Sunter et al., 1979). Differentiated cells are assumed to be in G_0 phase and never divide. There are simply ‘proliferative’ and ‘non-proliferative’ cells in our model. There is no distinct population of immortal stem cells, as their inclusion necessarily prevents the occurrence of monoclonal conversion (van Leeuwen et al., 2009; Fletcher et al., 2012).

When a cell enters mitosis, as determined by its cell-cycle model, a new cell-centre is placed a distance 0.1 cell diameters away from the parent in a random direction. We do not include cell growth explicitly in the model; in order to prevent cells from moving apart abruptly during mitosis, we let the equilibrium length of the spring connecting parent and daughter cell increase linearly from 0.1 to 1 during the M phase of the cell cycle. The equilibrium length of all other springs that connect to these cells remains 1 during this time.

In order to study separately the effects of mutations affecting proliferation and cell-substrate adhesion, we decouple them by

using simple models for each, as described below. Throughout this study, we assume that there is an initial mutant cell that produces mutant progeny, and that no other mutation occurs over the timescale of monoclonal conversion. Thus we neglect the probability of another mutant population entering the crypt during a given simulation.

2.3. Modelling changes to adhesion

Experimental results obtained by Sansom et al. (2004) indicate that mutations in the Wnt pathway influence cell migration. It is thought that this effect may be due to changes in cell-cell adhesion since β -catenin forms a bridge between adherens junctions and the cell cytoskeleton (Harris and Peifer, 2005).

Based on previous theoretical work (van Leeuwen et al., 2007), we hypothesise that cell-cell adhesion for mutant cells may differ from that of wild-type cells by up to 10-fold, and we consider $\alpha \in [0.3, 10]$. In reality a ten-fold increase in β -catenin may not cause a correspondingly large increase in adhesion, as other factors such as the availability of E-cadherin could become rate-limiting. Thus our chosen range is likely to include (and extend beyond) those values of α_i that are physiologically realistic; we emphasise here that we are focusing on the qualitative effects of changes to adhesion on mutant behaviour.

2.4. Modelling changes to proliferation

As noted in Section 1, certain mutations in the Wnt pathway enable proliferation to occur regardless of the level of the external Wnt stimulus (Sansom et al., 2007). Thus a disruption to the Wnt pathway may enable a mutant cell to continue to divide when exposed to a Wnt stimulus that inhibits proliferation in a wild-type cell. In this study we hypothesise that such disruption occurs to varying degrees according to the severity of the mutation. In more detail, we generate different mutant cells by varying the Wnt threshold W_{thr} that defines the proliferation ceiling y_{thr} , allowing the latter to vary from 30% to 100% of the crypt height. Note that the top of the crypt $y=h$, above which cells are sloughed, remains fixed regardless of the value of y_{thr} . Thus we use different height-dependent proliferation rules to investigate the influence of spatially dependent proliferation on the likelihood of a mutant population dominating a crypt.

2.5. Implementation

We have used Chaste, an open-source computational biology software library, to perform our simulations. The software implementation of the crypt model is discussed in Pitt-Francis et al. (2009), and the code used to generate the results presented in this paper is available as an open-source download from www.cs.ox.ac.uk/chaste.

Initially the crypt is set up with the dimensions discussed in Section 2.1 and allowed to evolve to a quasi-equilibrium state in which the mean number of cell divisions is equal to the mean number of cells sloughed from the crypt in any time period. In each of our simulations we ensure that the crypt is in such a quasi-equilibrium before introducing a mutant cell.

Individual clones in each simulation are tracked as follows: each cell is initially assigned a unique ‘ancestor index’ (an integer denoting its initial node index in the mesh suffices for this); this label is inherited by all of that cell’s progeny; we then evolve the crypt until all cells in the crypt have the same ancestor index. At this time the crypt has become monoclonal, i.e. all cells are either wild-type or all cells are mutant.

For simulations of mutant clones, we introduce mutant cells by randomly labelling a single cell in one of three height bands; in

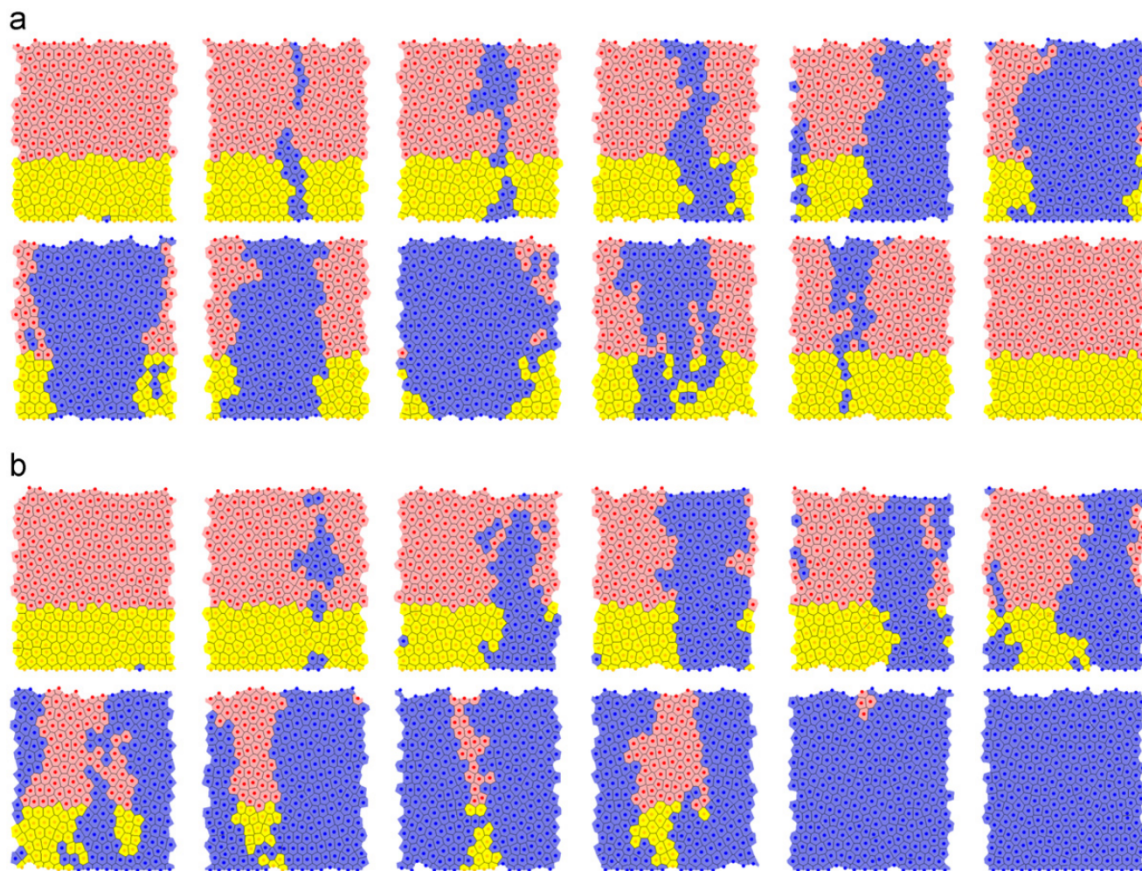


Fig. 3. Evolution of a mutant population within a crypt. In (a) a mutant population is swept out of the crypt, and in (b) a mutant population dominates the crypt. A single mutant cell is introduced into the base of a crypt in quasi-equilibrium. Snapshots are shown for every 100 h (~ 4 days or crypt renewal time) thereafter, going left to right then top to bottom, with the final snapshot at 1200 h (50 days). Here the ‘mutant’ population retains the same adhesion parameter ($\alpha = 1$) and proliferative ceiling ($y_{\text{thr}} = 35\%$) as healthy cells, and thus the mutation may be thought of as a neutral label. Red cells are differentiated, yellow cells are proliferating transit cells, and blue cells denote both proliferating and differentiated cells in the mutant clonal population. Domination such as that shown in (b) occurred in 500/10129 simulations in a ‘wild-type’ crypt. (For interpretation of the references to color in this figure caption, the reader is referred to the web version of this article.)

the bottom 5% of the crypt, in the bottom 5–10% and in the bottom 10–15% — approximately corresponding to vertical cell positions 1, 2 and 3 (the reason no mutations are introduced higher than this will become clear in the results section). Mutant cells are given a particular proliferation ceiling y_{thr} (35% of the crypt height for ‘wild type’ and between 30% and 100% of the crypt height for mutants with altered proliferation). Mutant cells are also given an adhesion parameter α of between 0.5 and 10, where $\alpha = 1$ for ‘wild-type’, as discussed above.

The simulation continues until the mutant population is swept out of, or dominates, the crypt, and we record the time at which the first of these events happens. Examples of typical simulations in which a mutant cell is introduced are shown in Fig. 3. In Fig. 3(a) the mutant clone is ‘swept out’ of the crypt, whilst in Fig. 3(b) the mutant clone ‘dominates’ the crypt. In this case the only difference between the simulations is the choice of initial labelled cell.

Due to the stochastic nature of the model, multiple simulations are needed to estimate the probability of a mutant cell taking over the crypt. A different initial condition is required for each simulation (due to the high number of simulations, even randomly mutating different cells in the same spatially organised crypt would lead to replicated runs). If a simulation ends with wild-type domination, then we re-use the final state of the crypt as an initial condition for our next simulation, as it has approximately the wild-type quasi-equilibrium cell density. However, if the simulation ends with mutant domination (no wild type cells remain), then the cell density in the crypt may be higher than

under wild-type conditions. Therefore, to obtain a new starting point for our next simulation, we discard the final crypt condition, re-use our original quasi-equilibrium state, and evolve it for a random duration ($\sim U(0,50)$ h) to gain a new initial condition.

We note that in order to build up statistical distributions, rather than simply show a ‘typical’ simulation result, the total amount of simulated ‘crypt time’ for this study was over 8×10^7 h (9000 years). The number of realisations for each choice of parameter values accompanies each result.

3. Results

Given that the crypt model replicates experimentally observed patterns of proliferation, migration and turnover rates (van Leeuwen et al., 2009), we concentrate on model predictions which follow from tracking its clones. We present results showing monoclonal conversion in wild-type crypts in Sections 3.1–3.3, and results for mutated cells in Sections 3.4–3.7.

3.1. Monoclonal conversion occurs in all simulations

In this section we study the process of monoclonal conversion by running multiple crypt simulations, as described in Section 2.5, in the absence of any mutation. In each case we track the progeny of each initial cell and stop the simulation as soon as the crypt becomes monoclonal, and all cells in the crypt have the same ancestor.

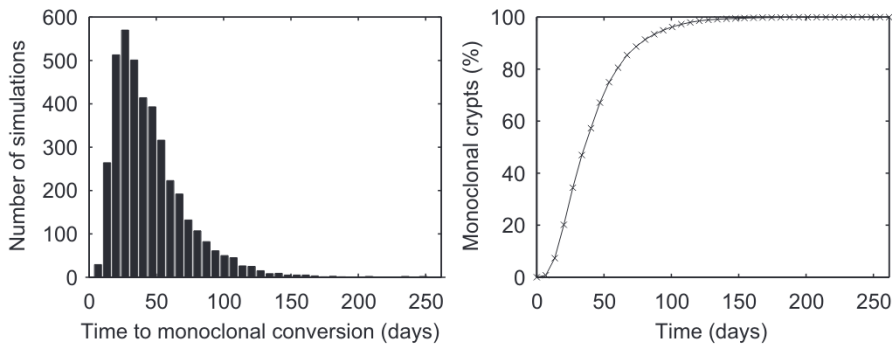


Fig. 4. Time to monoclonal conversion. Left: as a histogram, right: as a cumulative distribution function. Results shown are from 4000 simulations of a wild-type crypt, which always becomes monoclonal. Parameter values for these (and following) simulations are as discussed in Sections 2.1 and 2.2.

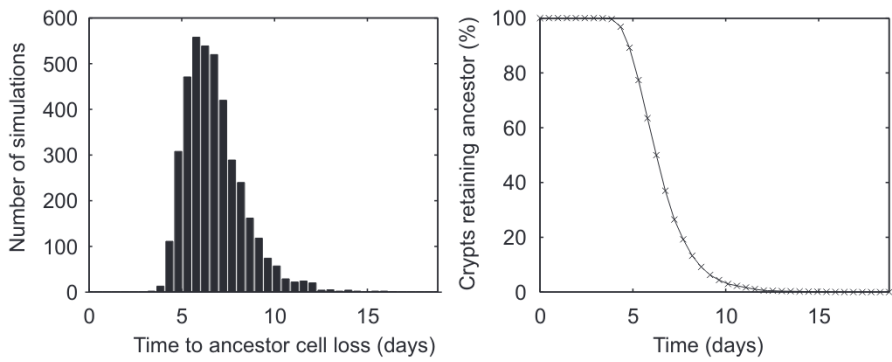


Fig. 5. Left: histogram of times at which the ancestor cell leaves the crypt. Right: times as a cumulative distribution function. Results shown are from 4000 simulations of a wild-type crypt.

In Fig. 4 we present a histogram from 4000 simulations summarising the times at which the crypts first become monoclonal. Monoclonal conversion was found to occur in each simulation, given sufficient time. The time taken for this to occur did not exceed 6040 simulated hours (≈ 36 weeks) for the 4000 simulations we performed. The reason that monoclonal conversion occurs in each simulation is that in our model, the crypt follows a pattern of neutral drift dynamics, whereby clonal populations expand and contract at random until they either take over the crypt or they are lost. This property of crypts has recently been confirmed experimentally by Lopez-Garcia et al. (2010). The process of neutral drift dynamics ensures a population that is of constant size on average, and leads to ever fewer yet larger clonal populations and a drift toward monoclonality (Snippert et al., 2010).

3.2. There are no immortal stem cells

The process of monoclonal conversion does not require that the cell which gave rise to the entire population remains in the crypt. We used data from the 4000 simulations described above to predict the time at which the original ancestor cell (the cell which at $t=0$ contained the ‘ancestor index’) is swept out of the crypt. In Fig. 5 we present a histogram and cumulative distribution function for the time at which the original ancestor cell that led to the dominant clone is lost from a crypt. Note that the timescale over which this process occurs is faster than that for monoclonal conversion. In these simulations, the ancestor cell was always expelled from the crypt before the crypt became monoclonal.

3.3. Dominant clones originate at the base of the crypt

In this section we introduce a ‘neutral’ mutant (or ‘labelled’ clone), with the same properties as the wild-type cells, such as those shown in Fig. 3, by simply labelling an existing cell and

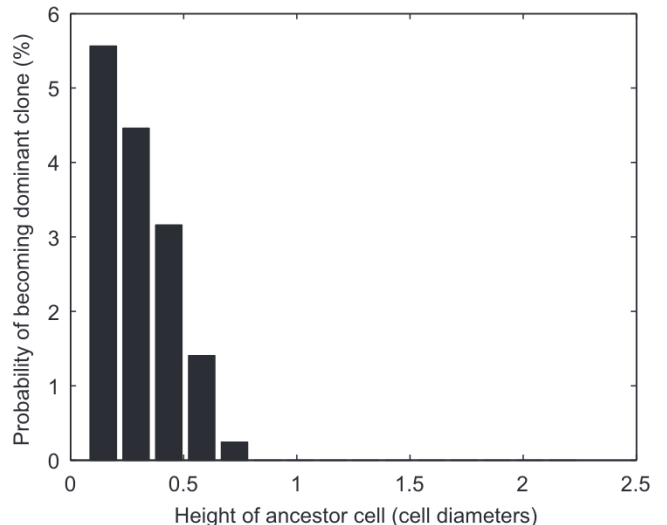


Fig. 6. Probability of the progeny of a cell labelled with a neutral mutation becoming the dominant clone as a function of height up the crypt. Results were generated from 12,129 simulations, of which 500 resulted in the labelled population dominating the crypt.

tracking its progeny. Each simulation ends when the labelled clonal population dominates or is swept out of the crypt. We performed 12129 simulations, as described in Section 2.5, in order to obtain 500 for which the labelled population eventually dominates the crypt.

Fig. 6 summarises these results and shows how the probability that a labelled clone becomes dominant varies as we vary the distance from the crypt base at which the label is introduced. At the base of the crypt the likelihood of becoming the dominant

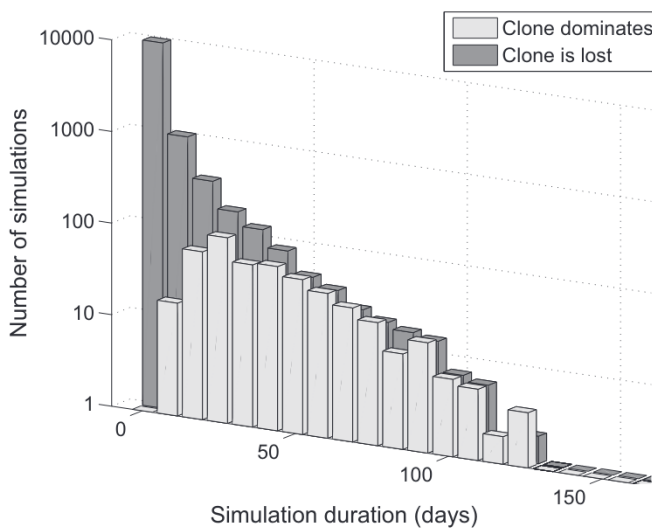


Fig. 7. Histogram of the durations of crypt simulations in which a neutral mutation is introduced. Simulations are run until the mutant population is ‘lost’ from (swept out of) or ‘dominates’ the crypt. Results were generated from 12,129 simulations, of which 500 resulted in the labelled population dominating the crypt. Note that a logarithmic (base 10) scale is used for the number of simulations.

clone approaches 6%, which is approximately equal to $1/N$, where N is the number of cells at the crypt base. This is the probability one would expect if only cells at the base of the crypt were capable of producing the dominant clone, and this were equally likely for all such cells. Labels introduced elsewhere in the crypt are quickly swept out: in over 12,000 simulations none of these neutral mutations introduced above 10% of the height of the crypt ever dominated. Fig. 7 shows a histogram of the duration of these simulations.

We see that the vast majority of simulations end when the mutant population is swept out of the crypt within 10 days of the initial mutation. Those mutants which dominate do so over a significantly longer period of time, up to 140 days after the initial mutation. In the case of longer simulations, in which the mutant population remains in the crypt for an extended period of time, the number of competing clones is typically reduced to 2, and for a ‘harmless’ mutation the probability of domination is approximately 50%. In such cases, the distribution of times for dominant clones to take over the crypt follows that shown in Fig. 4. This is in agreement with previous theoretical work by Fletcher et al. (2012). Thus we observe roughly equal numbers of ‘loss’ and ‘dominance’ for simulations ending at high durations.

These observations, in a wild-type setting, suggest that monoclonal conversion should not be thought of as a ‘one-off’ event, but rather as a continuous process. The clonal population giving rise to the entire population continuously shifts, in the battle to occupy the base of the crypt. In the following sections we use our model to investigate how different adhesive or proliferative properties associated with a particular mutation might accelerate this process.

3.4. Effect of varying mutant adhesion scaling parameter

In Fig. 8 we show how the likelihood of a mutant clone becoming dominant in the crypt depends on its adhesion scaling parameter α . As one might expect, mutant clones with increased cell–substrate adhesion are more likely to dominate. This is because in Eq. (1) the viscous drag force associated with adhesion is inversely proportional to velocity. The more adhesive mutant clones therefore move more slowly than the wild-type cells with which they are competing for space, although they proliferate at

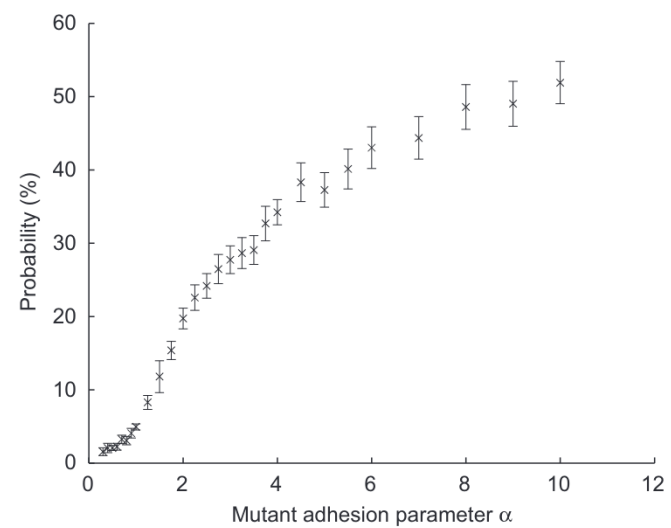


Fig. 8. Probability of a mutation introduced at the base of the crypt becoming the dominant clone, as the clone’s adhesion parameter α is varied from 0.3 to 10. In these simulations the mutation is assumed to affect cell–substrate adhesion but not proliferation ($y_{\text{thr}} = 35\%$). Error bars denote the 95% confidence interval for a binomial distribution with probability p , according to $p \pm z_{0.975} \sqrt{p(1-p)/n}$, where n is the number of simulations (600 for each value of α) and $z_{0.975}$ is the 97.5th percentile of a standard normal distribution. The probability for a wild-type cell is approximately 5% (at $\alpha = 1$).

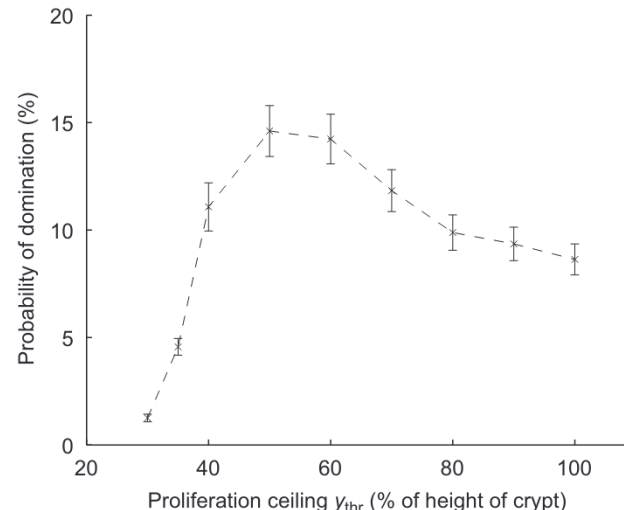


Fig. 9. Probability of a mutation introduced at the base of the crypt becoming the dominant clone, as its proliferation ceiling y_{thr} is varied. In these simulations the mutation is assumed to affect proliferation but not cell–substrate adhesion ($\alpha = 1$). Error bars denote the 95% confidence interval for a binomial distribution with probability p , according to $p \pm z_{0.975} \sqrt{p(1-p)/n}$, where n is the number of simulations and $z_{0.975}$ is the 97.5th percentile of a standard normal distribution. Variable numbers of simulations were performed until 500 dominations occurred (at least 3000 simulations) for each proliferation ceiling. For comparison, the probability for a wild-type cell to become the dominant clone is approximately 5% (at $y_{\text{thr}} = 35\%$).

the same rate. For low and intermediate levels of mutant cell–substrate adhesion, the associated advantage depends approximately linearly on the adhesion parameter, this relationship is discussed further in Section 3.6.

3.5. Effect of varying mutant proliferation ceiling

As described in Section 2.2, cells are assumed to proliferate between the base of the crypt and a given proliferation ceiling

y_{thr} set to be 35% of the height of the crypt for wild-type cells. We performed simulations for mutant cells, varying y_{thr} in the range 30% to 100% of the height of the crypt. In Fig. 9 we present results, showing how the likelihood of a mutant clone taking over the crypt changes as y_{thr} varies in this range.

As noted in Section 3.3, only those mutations occurring within one or two cell diameters of the crypt base can become established. In the simulations considered in the previous section, the difference between wild-type and mutant cell behaviour is only apparent some distance up the crypt. Therefore we may expect y_{thr} to have little effect on a mutant clone's probability of domination. However, as Fig. 9 shows, we instead find that the probability of domination increases as y_{thr} increases in the range $30\% < y_{\text{thr}} < 60\%$, and attains a maximal value when $y_{\text{thr}} \approx 50\%$, before asymptotically decreasing to a value of around 9% at $y_{\text{thr}} = 100\%$.

To investigate this behaviour further we decomposed our simulations into two groups: those in which the mutant population dominates the crypt and those in which it is swept out. We recorded the mean vertical component of forces per unit time experienced by cells at the base of the crypt, averaged over all simulations in each group. These results are presented in Fig. 10 and reveal the nonlocal influence of cells proliferating higher up the crypt: the increased levels of proliferation increase the number of cells in the crypt. This creates a higher cell density and therefore larger forces between cells. These forces propagate to the base of the crypt, since this is the only fixed boundary

against which cells may 'push'. In simulations where the mutant clone dominates, mutant cells at the crypt base experience a higher mean vertical force than wild-type cells, which acts preferentially to keep them 'in the stem cell niche'. In simulations where a wild-type clone dominates, the reverse is true. However, note that in both simulation groups, the mean vertical force on cells at the base of the crypt increases in magnitude as the proliferation ceiling y_{thr} increases.

Based on these results, we postulate the following mechanism to explain the results presented in Fig. 9. When a mutant clone continues to proliferate to heights slightly above those of wild-type cells, increased proliferation occurs directly above the mutant clone's position on the crypt base, and bestows a competitive advantage upon it by 'pushing it down'. By contrast, when a mutant clone proliferates throughout the crypt, the clone begins to spread laterally in the upper portion of the crypt where the wild-type cells do not proliferate. The resulting increased downward vertical forces act upon both the mutant cells, and a portion of the wild-type cells at the crypt base, providing a strong advantage not only to the mutant cells, but also to nearby wild-type cells. A schematic of this mechanism is depicted in Fig. 11.

3.6. Comparison with simplified one-dimensional model

To investigate further the relationship between the mutant adhesion parameter α , the proliferation ceiling y_{thr} and the probability of crypt domination, we may compare our results to

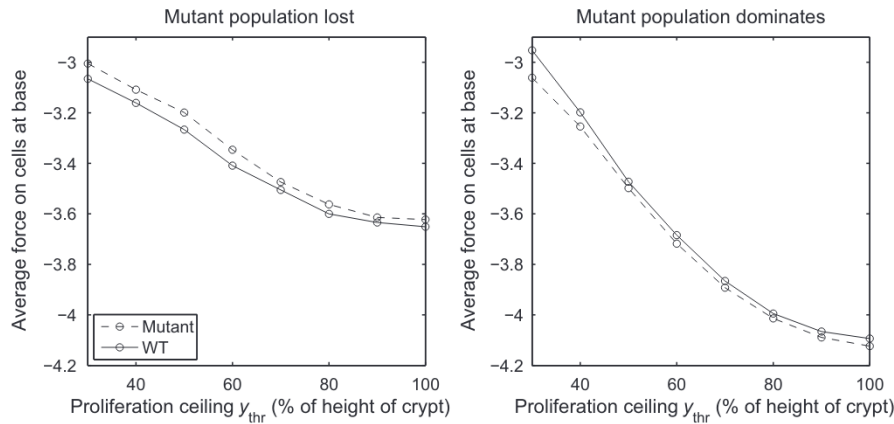


Fig. 10. Left: mean vertical component of the force per unit time on cells at the base of the crypt in simulations in which a mutant population with altered proliferation ceiling ($\alpha = 1$) is swept out of the crypt, where the average is taken over a variable number of simulations (at least 2500) for each value of y_{thr} . Right: mean vertical component of the force per unit time on cells at the base of the crypt in simulations in which a mutant population with altered proliferation ceiling ($\alpha = 1$) dominates the crypt, where the average is taken over 500 simulations for each value of y_{thr} .

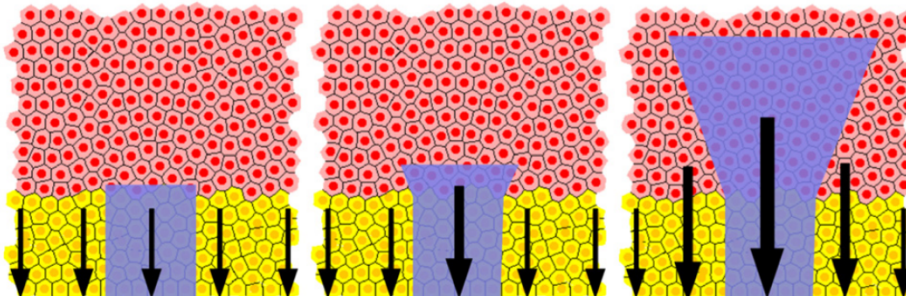


Fig. 11. A schematic of the mechanism by which proliferative ceiling relates to probability of domination, with size of forces (generated by proliferation and increased cell density) represented by size and thickness of arrow. Left: mutant clone proliferates to same height as wild-type cells. Middle: mutant clone proliferates higher than wild-type cells, and causes an increased vertical force above the mutant clone. Right: mutant clone proliferates to the top of the crypt, spreads laterally and causes an increased vertical force on the mutant clone and its wild-type neighbours. Note that the areas shaded blue represent average behaviour of a mutant clone, rather than the result of a single simulation. (For interpretation of the references to color in this figure caption, the reader is referred to the web version of this article.)

those obtained using a simple stochastic model that tracks the dynamics of a mutant cell introduced at the crypt base. This model is based on the work of Komarova (2007), and is a one-spatial-dimension generalisation of a mass-action Moran birth-death process. We note that a similar modelling framework has been used by Nowak et al. (2003) to understand the effect on the rate of somatic evolution of a linear spatial architecture. Here we are interested in the circumference of the base of the crypt, since we have already established that the probability of dominant mutations occurring above this region is negligible. We shall assume for simplicity that once a mutant population occupies the entirety of the bottom row of the crypt, it will dominate the crypt with probability one.

We assume that cells in the bottom row of the crypt are aligned along a regular grid, at locations $1, \dots, N$ (where $N \approx 16$, as discussed in Section 2.1). We impose periodic boundary conditions, so that locations 1 and N are neighbours, and make the simplifying assumption that the number of cells in this row remains constant over time. We assume that cells are removed at random from this row, due to mitotic forces propelling them up to the next row. Whenever a cell is removed, a division event occurs, with a daughter cell being generated by one of the cells that was adjacent to the removed cell.

We assume that there is an initial mutant cell, which produces mutant progeny. As in the rest of this study, we assume that no other mutation occurs over the timescale of interest. As we are interested in the probability of mutant domination, we only need take into account those changes in configuration that affect the number of mutant cells. Note that in this model, a mutant colony that originated as one cell can only occupy adjacent positions; in the cell-based model this is not enforced, but is usually the case. We let P_{exp}^l and P_{exp}^r denote the probabilities that a cell removal/division event results in a mutant population (of size greater than one) expanding to the left and right, respectively, and let P_{con}^l and P_{con}^r denote the probabilities that the population contracts to the left and right, respectively. We also let P_{ext} denote the probability that a mutant population of size one becomes extinct following a cell removal/division event. The mutant population differs from the wild-type population in its *relative fitness* (r). This relative fitness determines how much more likely a mutant population is than the wild-type population to expand to fill a gap left by an extinction, such that the probabilities of expansion, contraction and extinction are given in terms of r and N by

$$P_{\text{exp}}^l = P_{\text{exp}}^r = \frac{1}{N} \frac{r}{1+r}, \quad (2)$$

$$P_{\text{con}}^l = P_{\text{con}}^r = \frac{1}{N} \frac{1}{1+r}, \quad (3)$$

$$P_{\text{ext}} = \frac{1}{N}. \quad (4)$$

Whilst simplified models are more amenable to mathematical analysis, it is often not immediately clear how their system parameters relate to experimentally accessible quantities. The results of our cell-based model simulations offer an opportunity to examine what relationship, if any, there may be between the mutant fitness r in this simplified model and the two physical properties that vary for mutants in our cell-based model, namely the adhesion parameter α and proliferation ceiling y_{thr} .

As detailed by Komarova (2007), we can envisage the dynamics of this model as a two-dimensional Markov chain $(X_n)_{n \geq 0}$. The state space of this Markov chain is given by $S = \{1, \dots, N\}^2 \cup \emptyset$, where \emptyset corresponds to the extinction of the mutant population. The state $(i,j) \in S \setminus \emptyset$ characterises the positions of the leftmost and rightmost mutant cells, such that $1 \leq i \leq j \leq N$. This Markov chain has two absorbing states (Norris, 1997): the state $(1,N)$, in which the mutant

population has dominated the bottom row of the crypt; and the extinction state \emptyset . Let u_{ij} denote that probability that a mutant population starting at the state (i,j) , eventually reaches the state $(1,N)$, corresponding to mutant domination, then by applying the Markov property (Norris, 1997) it can be shown that

$$u_{ij} = u_{i-1,j} P_{\text{exp}}^l + u_{i+1,j} P_{\text{exp}}^r + u_{i,j-1} P_{\text{con}}^r + u_{i,j+1} P_{\text{con}}^l + u_{i,j} [1 - (P_{\text{exp}}^l + P_{\text{exp}}^r + P_{\text{con}}^r + P_{\text{con}}^l)], \quad (5)$$

for $1 < i < j \leq N$, and

$$u_{1,j} = u_{1,j-1} P_{\text{con}}^r + u_{1,j+1} P_{\text{con}}^l + u_{1,j} [1 - (P_{\text{con}}^r + P_{\text{con}}^l)], \quad 1 < j < N, \quad (6)$$

$$u_{i,N} = u_{i-1,N} P_{\text{exp}}^l + u_{i+1,N} P_{\text{exp}}^r + u_{i,N} [1 - (P_{\text{exp}}^l + P_{\text{exp}}^r)], \quad 1 < i < N, \quad (7)$$

$$u_{j,j} = u_{j-1,j} P_{\text{exp}}^l + u_{j,j+1} P_{\text{con}}^l + u_{j,j} [1 - (P_{\text{exp}}^l + P_{\text{con}}^l + P_{\text{ext}})], \quad 1 < j < N, \quad (8)$$

$$u_{1,1} = u_{1,2} P_{\text{con}}^r + u_{1,1} [1 - (P_{\text{con}}^r + P_{\text{ext}})], \quad (9)$$

$$u_{N,N} = u_{N-1,N} P_{\text{exp}}^l + u_{N,N} [1 - (P_{\text{exp}}^l + P_{\text{ext}})], \quad (10)$$

$$u_{1,N} = 1. \quad (11)$$

As discussed by Komarova (2007), periodicity of the spatial domain means that the quantities u_{ij} do not depend on the location of the mutant population, but only on its size. Let π_i denote the probability that the mutant population will dominate the bottom row starting from an initial patch of $(i+1)$ mutant cells, so that $\pi_i = \sum_{|I|=k=i+1} u_{k,l}$. Then, summing the appropriate equations from (5)–(11), we obtain the following system of equations for $(\pi_0, \dots, \pi_{N-1})$:

$$(P_{\text{exp}}^r + P_{\text{con}}^r) \pi_i = P_{\text{exp}}^r \pi_{i+1} + P_{\text{con}}^r \pi_{i-1}, \quad 0 < i < N-1, \quad (12)$$

$$\left(P_{\text{exp}}^r + \frac{1}{2} P_{\text{ext}} \right) \pi_0 = P_{\text{exp}}^r \pi_1, \quad (13)$$

$$\pi_{N-1} = 1. \quad (14)$$

Solving this linear system, we deduce that $\rho(r)$, the probability that the progeny of a single mutant cell eventually take over the entire bottom row of the crypt, is given by

$$\rho(r) \equiv \pi_0 = \frac{2r^{N-1}(1-r)}{1+r+r^{N-1}-3r^N} \rightarrow \frac{1}{N} \text{ as } r \rightarrow 1. \quad (15)$$

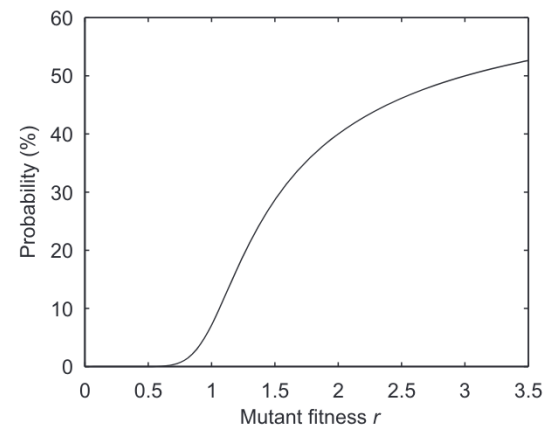


Fig. 12. Probability of a mutation introduced at the base of the crypt becoming the dominant clone, as a function of the clone's fitness r for $N=16$, according to a simpler stochastic model based on work by Komarova (2007).

The dependence of ρ on fitness r is shown in Fig. 12. Note there is a monotonic and saturating increase in the probability that a mutant dominates the base of the crypt as r increases.

Since the probability of domination observed in Fig. 12 increases monotonically, we can infer a value of r for a given domination probability. In Fig. 13 we plot the values of r that result in the domination probabilities observed in Figs. 8 and 9, when α and y_{thr} are varied. In each case we also plot a best-fit linear relationship between these data. As Fig. 13(a) shows, there is strong evidence of a linear relationship between r and α for the range of values considered in the simulations. This implies that in this simplified model, the concept of relative fitness can be used to describe the behaviour resulting from a mutant population with altered adhesion. In contrast, as shown in Fig. 13(b), no clear relationship exists between relative fitness at the crypt base and y_{thr} . We infer that in the case of altered proliferation the two-dimensional geometry of the crypt must be taken into account, when attempting to describe the relative fitness. The behaviour resulting from increased adhesion in the two-dimensional model appears to be captured well by increased fitness of the mutants at the crypt base.

3.7. Effect of varying mutant adhesion parameter, proliferation ceiling and height of mutation

Having investigated the effect of varying in turn each of the three mutant properties (height of the initial mutation, adhesion parameter and proliferation ceiling), in this section we consider how the probability of domination varies when a mutation affects all three properties.

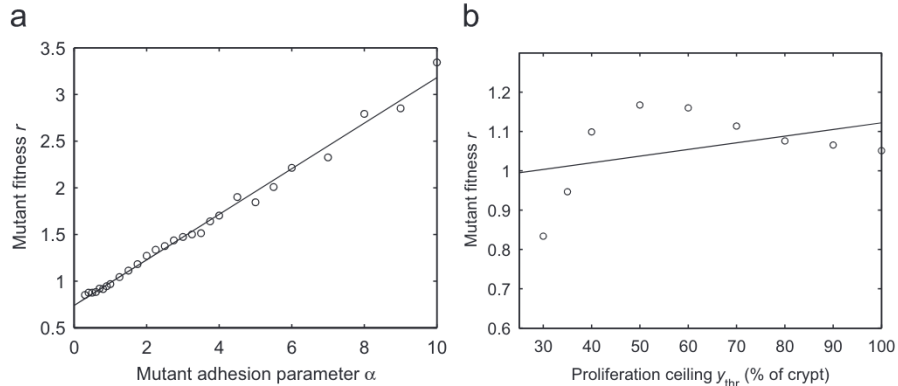


Fig. 13. Relationship between clone fitness r , and the increase in domination probability seen in our cell-based simulations (Figs. 8 and 9). The straight line fit in (a) is $r = 0.740 + 0.244\alpha$, in (b) $r = 0.945 + 0.00181y_{\text{thr}}$. (a) Fitness and mutant adhesion α and (b) fitness and proliferation ceiling y_{thr} .

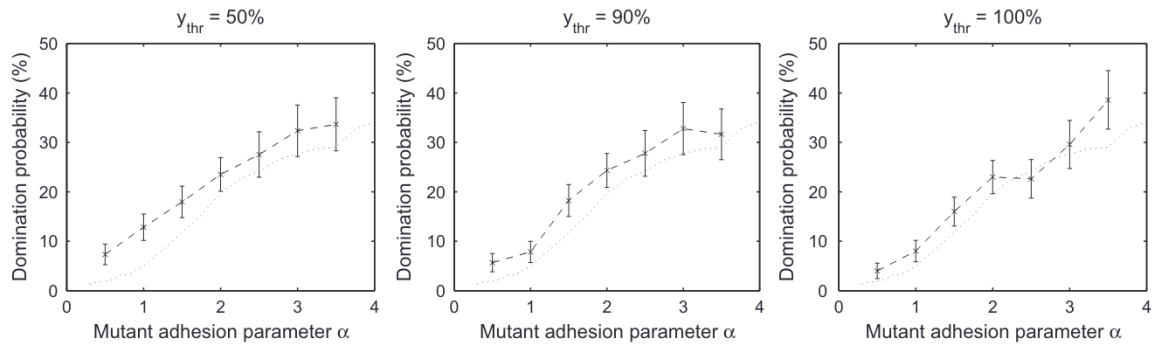


Fig. 14. Series of graphs showing how the probability that a mutation introduced at the base of the crypt becomes the dominant clone, varies with the clone's adhesion parameter, α . Error bars denote the 95% confidence interval for a binomial distribution probability p , according to $p \pm z_{0.975} \sqrt{p(1-p)/n}$, where n is the number of simulations (600 for each value of α) and $z_{0.975}$ is the 97.5th percentile of a standard normal distribution. Results for proliferation up to the following proportions of the crypt, left: 50%; middle: 90%; and right: 100%. Results for 35% (wild type), as shown in Fig. 8, are shown with a dashed line.

It is not computationally feasible to perform an exhaustive sweep of this three-dimensional parameter space. Therefore, guided by our findings in the previous sections, we restrict attention to certain values for each parameter. For the adhesion parameter α we consider variation from 0.5 to 3.5. For the proliferation ceiling y_{thr} , we examine four cases (wild-type 35%, 50%, 90% and 100% of the height of the crypt) chosen as they correspond to the heights to which common mutations in the Wnt pathway were expected to proliferate, in earlier theoretical work (van Leeuwen et al., 2009). These choices also include the maxima of Fig. 9. For the height of the initial mutation we consider the stratifications as above (for <5%, 5–10% and 10–15% of the height of the crypt). For all combinations of parameters the 10–15% band did not yield any clones that dominated the crypt, and hence these results are not shown.

Fig. 14 shows how, for different proliferation ceilings, the probability of domination varies with adhesion parameter for mutations introduced at the crypt base. We see that this probability is most sensitive to changes in adhesion, with the overall monotonic dependence on α being preserved for all values of y_{thr} considered. We would anticipate from Fig. 9 that those mutations with $y_{\text{thr}} = 50\%$ will have a larger probability of domination than the other mutations considered: this is indeed observed for $\alpha < 2$, but increased adhesion appears to dampen the advantage conferred by the optimal proliferation ceiling.

Fig. 15 shows how the probability of mutant domination varies with the height at which the initial mutation occurs, for different values of the mutant proliferation ceiling and adhesion parameter. In Fig. 9 we observed that the probability of domination increases and then decreases as the proliferation ceiling increases.

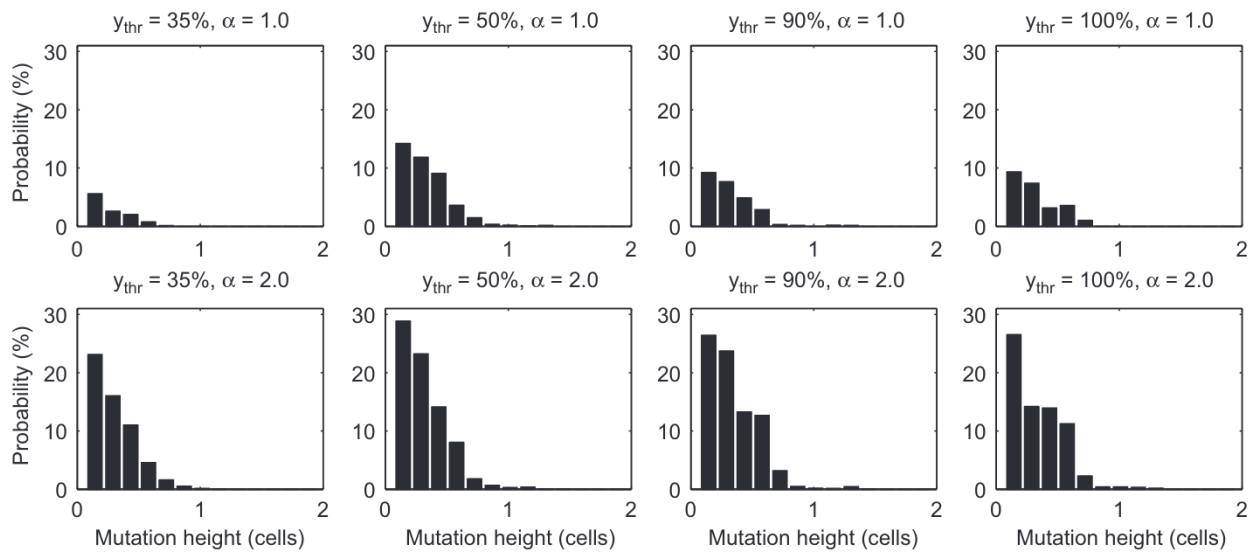


Fig. 15. Probability of a clone dominating the crypt, for varying choices of the initial mutation height. Results shown for four values of y_{thr} (35, 50, 90 and 100% of the height of the crypt) and for two different values of α (1.0 and 2.0). Each plot summarises the results from at least 350 simulations with dominant mutant clones, with given proliferation ceiling and adhesion parameter, and a corresponding proportion of simulations where the mutant clone is eliminated from the crypt (between 8000 and 18,000 simulations for each plot).

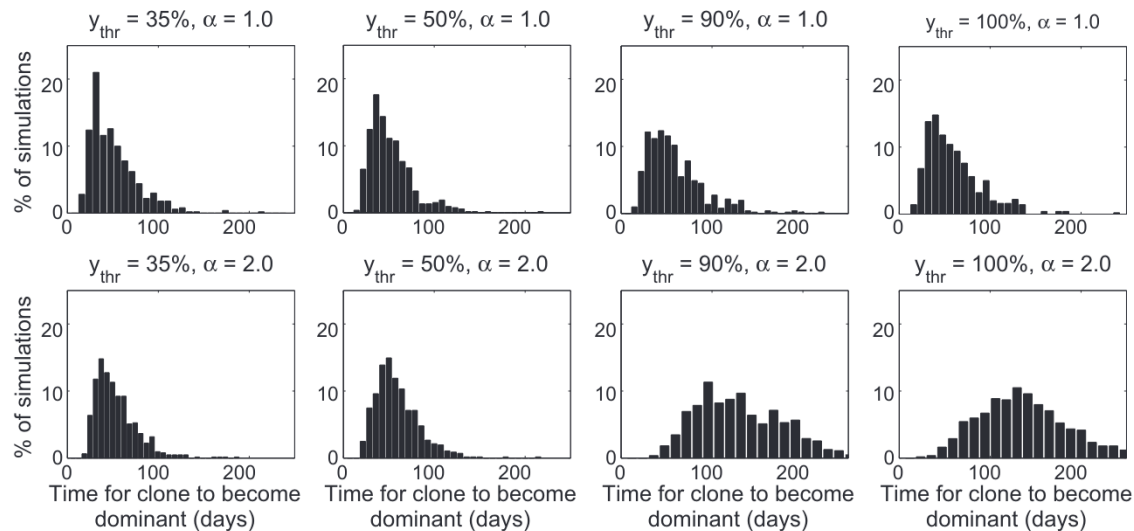


Fig. 16. Histograms of the duration of a dominant clone's persistence in the crypt. Results shown for four values of y_{thr} (35, 50, 90 and 100% of the height of the crypt) and for two different values of α (1.0 and 2.0). Each plot summarises the results from at least 350 simulations with dominant mutant clones, with given proliferation ceiling and adhesion parameter, and a corresponding proportion of simulations where the mutant clone is eliminated from the crypt (between 8000 and 18,000 simulations for each plot).

In the case of normal cell–substrate adhesion ($\alpha = 1$), in Fig. 15, we observe that this finding applies to mutations introduced throughout $0 \leq y \leq 1$. At a higher level of mutant cell–substrate adhesion ($\alpha = 2.0$), there is a slight increase in the probability of domination for mutations occurring above $y=0.5$. That is, there is a very small, but non-zero, probability of domination for mutations occurring up to $y=1.5$. Despite large variations in the probability that a mutant clone becomes dominant, the finding that it must occur at, or very close to, the base of the crypt is robust to changes in adhesion and proliferation ceiling.

In Fig. 16 we present histograms of the time taken for successful mutants with altered cell–substrate adhesion and proliferation to dominate the crypt. Using the same combinations of α and y_{thr} as those considered in Fig. 15, we find that the time taken for domination to occur increases slightly with y_{thr} when $\alpha = 1$, and more markedly when $\alpha = 2$. Thus the combination of

higher cell–substrate adhesion and greater vertical downward forces arising from a higher proliferation ceiling (as shown in Fig. 10) results in a longer period of competition before a successful mutant takes over the crypt.

4. Discussion

Intestinal homeostasis requires a coordinated programme of cell proliferation, migration and differentiation. The initiation of most colorectal cancers involves genetic alterations resulting in ‘over-activation’ of the Wnt signalling pathway. These alterations disrupt normal patterns of proliferation and cell–cell adhesion. Identifying the mechanisms by which a mutant population may colonise a crypt is therefore essential to understanding the origins of colorectal cancer.

In this paper, we have undertaken a computational study of how phenotypic variations, represented by differences in the proliferative and adhesive properties of individual cells, affect the likelihood that the progeny of a mutated cell will dominate a colonic crypt. We have employed a spatial model of a colonic crypt that distinguishes individual cells. The model couples the cell cycle and cell division with the mechanics of cell movement. By performing multiple simulations, varying not only the properties of the mutant cells but also the spatial location of the initial mutation, we have used the model to predict how the probability of domination depends on the properties of the mutant cells.

We began by considering the process of monoclonal conversion by running multiple crypt simulations in the absence of any mutation and, in each case, tracking the time taken for the progeny of one of the cells initially present to take over the entire crypt. Given sufficient time, monoclonal conversion always occurs in our model, since those cells that undergo symmetric division are following a pattern of neutral drift, as detailed by Snippert et al. (2010).

For some time there has been an ‘immortal strand’ (of DNA) hypothesis, which has been observed experimentally in some stem cell niches (Anversa et al., 2012). In this model the ‘stem cell’ attempts to retain original strands of DNA upon division, motivated by the fact that this strand is then not subject to copying errors. A prediction of our model is that monoclonal conversion does not require that the cell that gave rise to the entire population remains in the crypt. Indeed, in our simulations the timescale over which the original ancestor cell is lost from the crypt was found to be significantly shorter than that over which monoclonal conversion occurred. Our model does not include explicit individual stem cells, and indeed a new layer of complexity would have to be introduced to allow asymmetric division while retaining monoclonal conversion (cell-polarity, active migration, etc. are candidates).

We observed that the ability of a mutant clone to take over a crypt is extremely sensitive to the height at which the mutation occurs, with most mutants being swept out of the crypt due to the turnover and movement of normal cells up the crypt axis. In particular, ‘neutral’ mutations introduced more than one or two cells above the base of the crypt were unable to fixate within the crypt.

The probability of domination was found to be strongly affected by the extent to which mutations alter cell–substrate adhesion, represented in our model by the adhesion parameter α . This probability rises from approximately 6% for a neutral mutation at the crypt base to about 40% for a mutation characterised by a five-fold increase in cell–substrate adhesion.

We found that the probability of domination is only weakly influenced by disruption of control of cell proliferation associated with signalling cues such as Wnt, these being represented in our model by changes in the proliferation ceiling, y_{thr} . We obtained a counter-intuitive result, in which the probability of domination attains a maximum value of 15% with a proliferation ceiling around 50–60% of the height of the crypt (assuming no change in adhesion), the probability of domination decreasing for larger values of y_{thr} . We hypothesise that this behaviour arises due to an increase in the mean vertical component of the force per unit time on cells at the crypt base, which arises due to elevated levels of proliferation further up the crypt. We suggest that the associated increase in compression confers a competitive advantage on mutant cells, but that the lateral spread that occurs as cells move up the crypt causes this advantage to diminish when $y_{thr} > 60\%$.

We also compared our simulation results with those from a simple 1D stochastic model of the population dynamics at the base of the crypt. In the case of altered adhesion, we found a linear relationship between mutant cell–substrate adhesion in our cell-based model and mutant ‘fitness’ in the simplified model. In contrast,

when the proliferation ceiling was varied, our results indicate that the cells higher up the crypt may have a nonlocal effect on cells at the base, altering the probability of mutant cell domination. In more detail, when considering the case of a mutant with altered adhesion, a one-dimensional model of the crypt base accurately captures the competition between normal and mutant clones; while in the case of a mutant with altered proliferation, a two-dimensional model that accounts for distance from the crypt base and circumferential position is required.

In this study we have considered a highly simplified model of cell proliferation, in which all cells towards the crypt base experience a sufficiently high Wnt stimulus that they progress through the cell cycle, regardless of their size or degree of compression. Some experimental evidence indicates a more complex pattern of cell proliferation, in which cells located at the base of the crypt proliferate more slowly than those further up (Wright and Alison, 1984b). Further work is needed to determine whether the reduction in the average rate of cell proliferation at the crypt base is due to mechanical compression or the presence of (non-cycling) differentiated Paneth cells (Sato et al., 2010).

Two hypotheses have been advanced to explain the process whereby adenomatous cells populate neighbouring crypts to form polyps. The ‘top-down’ theory proposes that the first mutant cells appear near the top of a crypt, where they effect a proliferation-driven, downward invasion (Lamprecht and Lipkin, 2002; Komarova and Wang, 2004). Alternatively, under the ‘bottom-up’ hypothesis, mutant cells originate at the crypt base, migrate upwards, colonizing the crypt (Preston et al., 2003), which subsequently undergoes crypt fission. The existence of experimental results which support each hypothesis (Maskens, 1979; Shih et al., 2001; Wong et al., 1999) suggest that both occur, with bottom-up invasion of crypts (and crypt fission) being the earlier event in carcinogenesis (Deheragoda and Wright, 2006).

According to our model, even mutants with unlimited proliferative ability, or those with significantly increased cell–cell adhesion, would not colonise the entire crypt unless the mutation occurs near the crypt base. We conclude that bottom-up invasion is more likely to occur than top-down invasion, and that top-down invasion requires more dramatic mutations that for example prevent cells from being ‘sloughed off’ the top of the crypt.

To describe cell movement, we have used a simple model of mechanical relaxation based on linear springs. Since the tissue-level behaviour of cell-centre models is not thought to be strongly affected by the spring model used for mechanics (Pathmanathan et al., 2009), we anticipate that our predictions, that monoclonal conversion requires mutations to occur at the base of the crypt, will be robust to the choice of cell-centre model.

One might expect that, in simulations where the mutant population has a very high level of cell–substrate adhesion, the rate of cell movement out of the crypt may be insufficient to match the rate at which cells are introduced from mitosis. This was not observed at the levels of cell–substrate adhesion considered in this study. If this were the case, rather than reaching a quasi-equilibrium, the number of cells in the crypt may increase exponentially, rapidly reaching physically unrealistic levels. This behaviour has been analysed in a coarse-grained continuum model of an intestinal crypt by Murray et al. (2011).

Simulations of cell–vertex or continuum models have revealed that top-down invasion can occur if adhesive effects are very strong (Osborne et al., 2010). This behaviour is unlikely to occur *in vivo* due to ‘contact inhibition’ and/or buckling of the basement membrane and subsequent crypt deformation.

The biological mechanism through which shear stress affects the expression of key components in the Wnt signalling pathway has recently been elucidated (Avvisato et al., 2007; Whitehead

et al., 2008); and a recent theoretical model by Basan et al. (2010) proposed a mechanism through which contact inhibition affects the concentrations of β -catenin and E-cadherin within the cytoplasm. The inclusion of a more detailed description of mechanical feedback on cells' transcriptional and adhesive behaviour therefore offers a promising direction for future work.

In addition, it is becoming increasingly clear that mutations affecting individual proteins can cause significant alterations in cell function as a result of crosstalk between signalling pathways. This was illustrated by the identification of a positive feedback loop present between the Wnt pathway and the extracellular signal regulated-kinase pathway (Kim et al., 2007). This work highlights the need for more accurate models of the signalling networks underlying cell proliferation and adhesion, as well as an awareness of the extent to which model predictions are robust to the presence of crosstalk between these networks.

A simplification we have made in the present study concerns the geometrical description of the crypt. While our simplified geometry overestimates the number of cells at the base of the crypt, we envisage that the qualitative nature of our predictions will be preserved when the more detailed geometries are considered (see Buske et al., 2011; Fletcher et al., 2012), although quantitative predictions for persistence times and probabilities of domination may vary.

In order to determine how a proliferative advantage bestowed upon mutant cells within a crypt translates into an increased probability of domination, and how this probability varies with the location of the initial mutation, a large number of model simulations were required. This computational intensity is a problem intrinsic to discrete stochastic models. The problem would be compounded where we to include a more detailed model of how mutations in the Wnt pathway affect proliferation and adhesion at the cellular level, such as that proposed by van Leeuwen et al. (2007). Our simplified geometry and description of cell behaviour has enabled us to perform the large number of *in silico* experiments needed to generate, for the first time, statistical distributions for crypt domination events. One resolution of the problem is to develop coarse-grained models, which replicate the essential features of the original model, but to which established mathematical techniques such as asymptotic and bifurcation analysis may be applied. This remains an area of current research (Fozard et al., 2010; Murray et al., 2010), the key difficulty being how to retain in such coarse-grained models the necessary level of detail and spatial resolution to represent mutations in single cells.

A natural extension is to model the curved, three-dimensional geometry of the crypt in a sufficiently computationally efficient manner that such statistics may still be obtained, and preliminary work in this direction has been undertaken by Dunn et al. (2012b) in modelling the generation of crypt curvature. In this work we have only considered a single crypt. It is becoming clear that inter-crypt interactions may be significant in the establishment of lesions such as colonic adenomas (see Humphries and Wright, 2008 and references therein). A natural next step is to consider the processes by which a mutant clonal population, having taken over a single crypt, invades and dominates neighbouring crypts. This may require further mutations, for example to prevent sloughing at the top of the crypt. Equally a three-dimensional model of the crypt that accounts for interactions with the surrounding stroma, and allows for deformation of the epithelium, would permit investigation of the impact of such events on colorectal cancer. These remain avenues for future research.

Acknowledgments

The authors gratefully acknowledge financial support from the EPSRC awarded to AGF and GRM as part of the Integrative Biology

programme (GR/572023/01). GRM is supported by a GlaxoSmithKline Plc Grants and Affiliates award. AGF is funded by the EPSRC and Microsoft Research, Cambridge through Grant EP/I017909/1 (www.2020science.net). AGF and PKM acknowledge support from the BBSRC through grant BB/D020190/1. PKM was partially supported by a Royal Society Wolfson Research Merit Award. This publication was based on work supported in part by Award no. KUK-C1-013-04, made by King Abdullah University of Science and Technology (KAUST).

References

- Anversa, P., Leri, A., Kajstura, J., 2012. Biased dna segregation during stem cell division. *Circul. Res.* 110, 1403–1407.
- Avvisato, C., Yang, X., Shah, S., Hoexter, B., Li, W., Gaynor, R., Pestell, R., Tozeren, A., Byers, S., 2007. Mechanical force modulates global gene expression and β -catenin signaling in colon cancer cells. *J. Cell Sci.* 120, 2672–2682.
- Barker, N., van Es, J., Kuipers, J., Kujala, P., van den Born, M., Cozijnsen, M., Haegeman, A., Korving, J., Begthel, H., Peters, P., et al., 2007. Identification of stem cells in small intestine and colon by marker gene Lgr5. *Nature* 449, 1003–1007.
- Barker, N., Ridgway, R., van Es, J., van de Wetering, M., Begthel, H., van den Born, M., Danenberg, E., Clarke, A., Sansom, O., Clevers, H., 2008. Crypt stem cells as the cells-of-origin of intestinal cancer. *Nature* 457, 608–611.
- Basan, M., Idema, T., Lenz, M., Joanny, J., Risler, T., 2010. A reaction-diffusion model of the cadherin–catenin system: a possible mechanism for contact inhibition and implications for tumorigenesis. *Biophys. J.* 98, 2770–2779.
- Boman, B., Fields, J., Cavanaugh, K., Guetter, A., Runquist, O., 2008. How dysregulated colonic crypt dynamics cause stem cell overpopulation and initiate colon cancer. *Cancer Res.* 68, 3304–3313.
- Bullen, T., Forrest, S., Campbell, F., Dodson, A., Hershman, M., Pritchard, D., Turner, J., Montrose, M., Watson, A., 2006. Characterization of epithelial cell shedding from human small intestine. *Lab. Invest.* 86, 1052–1063.
- Buske, P., Galle, J., Barker, N., Aust, G., Clevers, H., Loeffler, M., Lauffenburger, D., 2011. A comprehensive model of the spatio-temporal stem cell and tissue organisation in the intestinal crypt. *PLoS Comp. Biol.* 7, 1332–1336.
- Deheragoda, M., Wright, N., 2006. An update on the pathophysiology of the intestinal crypt. *Curr. Diagn. Pathol.* 12, 268–278.
- Dietrich, C., Scherwat, J., Faust, D., Oesch, F., 2002. Subcellular localization of β -catenin is regulated by cell density. *Biochem. Biophys. Res. Commun.* 292, 195–199.
- Drasdo, D., Loeffler, M., 2001. Individual-based models to growth and folding in one-layered tissues: intestinal crypts and early development. *Nonlinear Anal.—Theory* 47, 245–256.
- Dunn, S., Appleton, P., Nelson, S., Nähkne, I., Gavaghan, D., Osborne, J., 2012a. A two-dimensional model of the colonic crypt accounting for the role of the basement membrane and pericycral fibroblast sheath. *PLoS Comput. Biol.* 8, e1002515.
- Dunn, S., Fletcher, A., Chapman, S., Gavaghan, D., Osborne, J., 2012b. Modelling the role of the basement membrane beneath a growing epithelial monolayer. *J. Theor. Biol.* 298, 82–91.
- Edwards, C., Chapman, S., 2007. Biomechanical modelling of colorectal crypt budding and fission. *Bull. Math. Biol.* 69, 1927–1942.
- Fletcher, A., Breward, C., Chapman, S., 2012. Mathematical modeling of monoclonal conversion in the colonic crypt. *J. Theoret. Biol.* 300, 118–133.
- Fozard, J., Byrne, H., Jensen, O., King, J., 2010. Continuum approximations of individual-based models for epithelial monolayers. *Math. Med. Biol.* 27, 39–74.
- Gaspar, C., Fodde, R., 2004. APC dosage effects in tumorigenesis and stem cell differentiation. *Int. J. Dev. Biol.* 48, 377–386.
- Gregoriet, A., Clevers, H., 2005. Wnt signaling in the intestinal epithelium: from endoderm to cancer. *Genes Dev.* 19, 877–890.
- Harris, T., Peifer, M., 2005. Decisions, decisions: β -catenin chooses between adhesion and transcription. *Trends Cell Biol.* 15, 234–237.
- Humphries, A., Wright, N., 2008. Colonic crypt organization and tumorigenesis. *Nat. Rev. Cancer* 8, 415–424.
- Ilyas, M., 2005. Wnt signalling and the mechanistic basis of tumour development. *J. Pathol.* 205, 130–144.
- Johnston, M., Edwards, C., Bodmer, W., Maini, P., Chapman, S., 2007. Mathematical modeling of cell population dynamics in the colonic crypt and in colorectal cancer. *Proc. Natl. Acad. Sci. USA* 104, 4008–4013.
- Kaur, P., Potten, C., 1986. Effects of puromycin, cycloheximide and noradrenaline on cell migration within the crypts and on the villi of the small intestine. A model to explain cell movement in both regions. *Cell Prolif.* 19, 611.
- Kim, D., Rath, O., Kolch, W., Cho, K., 2007. A hidden oncogenic positive feedback loop caused by crosstalk between Wnt and ERK pathways. *Oncogene* 26, 4571–4579.
- Komarova, N., 2007. Loss-and gain-of-function mutations in cancer: mass-action, spatial and hierarchical models. *J. Stat. Phys.* 128, 413–446.
- Komarova, N., Wang, L., 2004. Initiation of colorectal cancer. *Cell Cycle* 3, 1558–1565.

- Lamprecht, S., Lipkin, M., 2002. Migrating colonic crypt epithelial cells: primary targets for transformation. *Carcinogenesis* 23, 1777–1780.
- Loeffler, M., Birke, A., Winton, D., Potten, C., 1993. Somatic mutation, monoclonality and stochastic models of stem cell organization in the intestinal crypt. *J. Theor. Biol.* 160, 471.
- Lopez-Garcia, C., Klein, A., Simons, B., Winton, D., 2010. Intestinal stem cell replacement follows a pattern of neutral drift. *Science* 330, 822–825.
- Maskens, A., 1979. Histogenesis of adenomatous polyps in the human large intestine. *Gastroenterology* 77, 1245.
- Meineke, F., Potten, C., Loeffler, M., 2001. Cell migration and organization in the intestinal crypt using a lattice-free model. *Cell Prolif.* 34, 253–266.
- Mirams, G., 2008. Subcellular Phenomena in Colorectal Cancer. PhD Thesis. University of Nottingham.
- Mirams, G., Byrne, H., King, J., 2010. A multiple timescale analysis of a mathematical model of the Wnt/β-catenin signalling pathway. *J. Math. Biol.* 60, 131–160.
- Morin, P., Sparks, A., Korinek, V., Barker, N., Clevers, H., Vogelstein, B., Kinzler, K., 1997. Activation of β-catenin-Tcf signaling in colon cancer by mutations in β-catenin or APC. *Science* 275, 1787–1790.
- Murray, P., Kang, J., Mirams, G., Shin, S., Byrne, H., Maini, P., Cho, K., 2010. Modelling spatially regulated β-catenin dynamics and invasion in intestinal crypts. *Biophys. J.* 99, 716–725.
- Murray, P., Walter, A., Fletcher, A., Edwards, C., Tindall, M., Maini, P., 2011. Comparing a discrete and continuum model of the intestinal crypt. *Phys. Biol.* 8, 026011.
- Nelson, W., Nusse, R., 2004. Convergence of Wnt, β-catenin, and cadherin pathways. *Science* 303, 1483–1487.
- Norris, J., 1997. Markov Chains. Cambridge University Press.
- Nowak, M., Michor, F., Iwasa, Y., 2003. The linear process of somatic evolution. *Proc. Natl. Acad. Sci. USA* 100, 14966–14969.
- Okamoto, R., Watanabe, M., 2004. Molecular and clinical basis for the regeneration of human gastrointestinal epithelia. *J. Gastroenterol.* 39, 1–6.
- Osborne, J., Walter, A., Kershaw, S., Mirams, G., Fletcher, A., Pathmanathan, P., Gavaghan, D., Jensen, O., Maini, P., Byrne, H., 2010. A hybrid approach to multi-scale modelling of cancer. *Philos. Trans. R. Soc. A* 368, 5013–5028.
- Pathmanathan, P., Cooper, J., Fletcher, A., Mirams, G., Murray, P., Osborne, J., Pitt-Francis, J., Walter, A., Chapman, S.J., 2009. A computational study of discrete mechanical tissue models. *Phys. Biol.* 6, 036001.
- Perez-Moreno, M., Jamora, C., Fuchs, E., 2003. Sticky business orchestrating cellular signals at adherens junctions. *Cell* 112, 535–548.
- Pinto, D., Gregoriet, A., Begthel, H., Clevers, H., 2003. Canonical Wnt signals are essential for homeostasis of the intestinal epithelium. *Genes Dev.* 17, 1709–1713.
- Pitt-Francis, J., Pathmanathan, P., Bernabeu, M., Bordas, R., Cooper, J., Fletcher, A., Mirams, G., Murray, P., Osborne, J., Walter, A., Chapman, J., Garny, A., van Leeuwen, I., Maini, P., Rodriguez, B., Waters, S., Whiteley, J., Byrne, H., Gavaghan, D., 2009. Chaste: a test-driven approach to software development for biological modelling. *Comp. Phys. Commun.* 180, 2452–2471.
- Potten, C., Booth, C., Hargreaves, D., 2003. The small intestine as a model for evaluating adult tissue stem cell drug targets. *Cell Prolif.* 36, 115–129.
- Powell, S., Zilz, N., Beazer-Barclay, Y., Bryan, T., Hamilton, S., Thibodeau, S., Vogelstein, B., Kinzler, K., 1992. APC mutations occur early during colorectal tumorigenesis. *Nature* 359, 235–237.
- Preston, S., Wong, W., Chan, A., Poulsom, R., Jeffery, R., Goodlad, R., Mandir, N., Elia, G., Novelli, M., Bodmer, W., et al., 2003. Bottom-up histogenesis of colorectal adenomas. *Cancer Res.* 63, 3819.
- Ross, M., Kaye, G., Pawlina, W., 2003. Histology: A Text and Atlas: With Cell and Molecular Biology. Lippincott Williams & Wilkins.
- Sansom, O., Meniel, V., Muncan, V., Phesse, T., Wilkins, J., Reed, K., Vass, J., Athineos, D., Clevers, H., Clarke, A., 2007. Myc deletion rescues Apc deficiency in the small intestine. *Nature* 446, 676–679.
- Sansom, O., Reed, K., Hayes, A., Ireland, H., Brinkmann, H., Newton, I., Batlle, E., Simon-Assmann, P., Clevers, H., Nathke, I., Clarke, A., Winton, D., 2004. Loss of Apc in vivo immediately perturbs Wnt signaling, differentiation, and migration. *Genes Dev.* 18, 1385–1390.
- Sato, T., van Es, J., Snippert, H., Stange, D., Vries, R., van den Born, M., Barker, N., Shroyer, N., van de Wetering, M., Clevers, H., 2010. Paneth cells constitute the niche for Lgr5 stem cells in intestinal crypts. *Nature* 469, 415–418.
- Shih, I., Wang, T., Traverso, G., Romans, K., Hamilton, S., Ben-Sasson, S., Kinzler, K., Vogelstein, B., 2001. Top-down morphogenesis of colorectal tumors. *Proc. Natl. Acad. Sci. USA* 98, 2640–2645.
- Snippert, H., van der Flier, L., Sato, T., van Es, J., van den Born, M., Kroon-Veenboer, C., Barker, N., Klein, A., van Rheenen, J., Simons, B., Clevers, H., 2010. Intestinal crypt homeostasis results from neutral competition between symmetrically dividing Lgr5 stem cells. *Cell* 143, 134–144.
- Sparks, A., Morin, P., Vogelstein, B., Kinzler, K., 1998. Mutational analysis of the APC/β-catenin/Tcf pathway in colorectal cancer. *Cancer Res.* 58, 1130–1134.
- Sunter, J., Appleton, D., Dé Rodriguez, M., Wright, N., Watson, A., 1979. A comparison of cell proliferation at different sites within the large bowel of the mouse. *J. Anat.* 129, 833–842.
- van de Wetering, M., Sancho, E., Verweij, C., de Lau, W., Oving, I., Hurlstone, A., van der Horn, K., Batlle, E., Coudreuse, D., Haramis, A., Tjon-Pon-Fong, M., Moerer, P., van den Born, M., Soete, G., Pals, S., Eilers, M., Medema, R., Clevers, H., 2002. The β-catenin/TCF-4 complex imposes a crypt progenitor phenotype on colorectal cancer cells. *Cell* 111, 241–250.
- van Leeuwen, I., Byrne, H., Jensen, O., King, J., 2007. Elucidating the interactions between the adhesive and transcriptional functions of β-catenin in normal and cancerous cells. *J. Theor. Biol.* 247, 77–102.
- van Leeuwen, I., Mirams, G., Walter, A., Fletcher, A., Murray, P., Osborne, J., Varma, S., Young, S., Cooper, J., Doyle, B., Pitt-Francis, J., Momtahan, L., Pathmanathan, P., Whiteley, J., Chapman, S.J., Jensen, O., King, J., Maini, P., Waters, S., Gavaghan, D., Byrne, H., 2009. An integrative computational model for intestinal tissue renewal. *Cell Prolif.* 42, 617–636.
- Whitehead, J., Vignjevic, D., Fütterer, C., Beaurepaire, E., Robine, S., Farge, E., 2008. Mechanical factors activate β-catenin-dependent oncogene expression in *apc1638n/+* mouse colon. *HFSP J.* 2, 286–294.
- Wong, W., Garcia, S., Wright, N., 1999. Origins and morphogenesis of colorectal neoplasms. *APMIS* 107, 535–544.
- Wright, N., Alison, M., 1984a. The Biology of Epithelial Cell Populations, vol. 1. Clarendon Press, Oxford.
- Wright, N., Alison, M., 1984b. The Biology of Epithelial Cell Populations, vol. 2. Clarendon Press, Oxford.

